IJCAT - International Journal of Computing and Technology, Volume 3, Issue 3, March 2016
ISSN : 2348 - 6090
www.IJCAT.org

Single Stage- Three Phase Grid Connected PV System Based on Current Source Inverter

[1]P.DEVANANDA BABJI (M.TECH)
Student

[2]M.CHANDRA SEKHAR M.Tech
Asst.Professor

[1,2] Lenora College of Engineering- Rampachodavaram

Abstract—**The current source inverter (CSI) has advantage of inherent boosting and direct output current contollability and short circuit protection capabilities over viltahe source converter. The cost and complexity of current source converter is less compared to voltage source inverter (VSI). This paper focuses on modeling, control, and stedy state and transient performance of a PV system based on CSI. It also performs a comparative performance evaluation ofVSI-based and CSI-based PV systems under transient and fault conditions. Analytical expectations are verfied using simulations in MATLAB software.**

Index Terms **photovoltaic (PV), modeling, fault, Control, current-source inverter (CSI), transient behavior**

I. INTRODUCTION

In recent years, photovoltaic (PV) systems have received unprecedented attention due to the concerns about adverse effects of extensive use of fossil fuels on the environment and energy security. Despite this high interest, grid-connected PV systems are still outnumbered by the power generation schemes based on oil, natural gas, coal, nuclear, hydro, and wind [1].

So far, PV systems of capacities on the order of tens of megawatts have been installed and interfaced to the grid mainly at the primary distribution level. PV system installations at the secondary distribution level are dominated by rooftop units with capacities on the order of a few kilowatts with no significant impact on the existing power systems. With the growing interest in solar energy and adoption of national policies in favor of green energy, a significant increase in the number of large size PV plants, with significant impact on the existing power grid is expected. The two main components of a PV system with potential for improvement are PV modules and power electronic inverters. PV modules

big way. Fortunately, a downward trend is clearly noticed in the price per watt of PV modules due to significant increase in the production of PV modules in different parts of the world. More specifically, in 1992, the price of a PV module was 4.4 7.9 USD per watt .The current market price is 2.6 3.5USD per watt[2].

The present practice in PV inverter mainly relies on voltage source inverter (VSI) topology which normally requires another stage of power electronic conversion for stepping up the voltage of the PV modules for a large-scale PV inverter.Reducing the cost and improving the robustness and performance of power electronic grid interface can further facilitate proliferation of PV systems in the power systems.The current-source inverter (CSI) has the potential of be-coming a preferred topology for interfacing a PV system to the ac power grid for the following reasons. 1) CSI provides a smooth dc - side current, which is a desirable feature for PV modules. 2) The energy storage element of a CSI has a longer lifetime than that of a VSI. 3) CSI has an inherent voltage boosting capability, which allows integration of PV panels of lower output voltages and reduces the requirements of the step-up interface transformer. 4) With the evolution of reverse-blocking (RB) IGBT switches, the series diodes will be eliminated, resulting in a considerable reduction in the cost and conduction losses. 5) The recent advancements in super-conductor

technology, which has led to the development of superconducting magnetic energy storage (SMES) systems, can considerably reduce the losses in the energy storage element of the CSI.

resistance and inductance of the distribution line are represented by R_g and L_g, respectively.Ps and Qs respectively, represent the active and reactive powers supplied by the PV system to the distribution system.

The breaker B_r is part of the protection system installed by the utility. The control structure proposed for the CSI-based PV system is composed of an outer current control loop designed to control the dc-side current and an inner current control loop responsible for controlling the current that is injected into the gird.

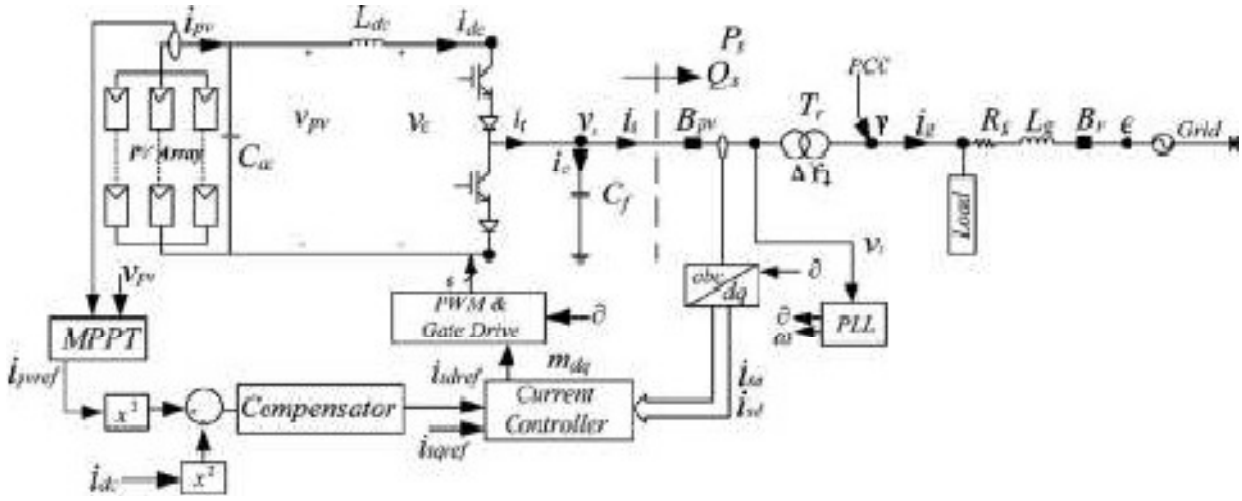

Fig. 1. Single-line diagram of the proposed threephase,single-stage, grid-connected PV system based on CSI.

The dc-side inductor L_{dc} filters out the ripples in the dc side current and allows its control. The ac-side of the inverter is interfaced with the primary side of the transformer T_r through a capacitive filter composed of three Y-connected capacitors C_f . The function of C_f is to absorb switching harmonics and produce clean sinusoidal current at the grid interface. Breaker B_{pv} is an integral part of the PV system and is provided to protect the PV system by isolating it when there is fault on the secondary side of the transformer T_r. The primary side of the transformer is delta-connected whereas its secondary side is star connected with a solidly grounded neutral point. The

A maximum power point tracker (MPPT) is employed to ensure that the PV array is operating at its maximum power. the dc-side current and an inner current control loop responsible for controlling the current that is injected into the grid. A maximum power point tracker (MPPT) is employed to ensure that the PV array is operating at its maximum power.

II. CHARACTERISTICS OF PV ARRAY

The PV array I-V characteristic is described by the following [1]:

$$i_{pv} = n_p i_{ph} - n_p i_{rs}\left[exp\left(\frac{q}{kT_cA}\frac{v_{pv}}{n_s}\right) - 1\right] \quad \text{.....1}$$

In (1), q is the unit charge,k the Boltzman's constant, A the p-n junction ideality factor, and T_c the cell temperature. Current i_{rs} is the cell reverse saturation current, which varies with temperature according to

$$i_{rs} = i_{rr}\left[\frac{T_c}{T_{ref}}\right]^3 exp\left(\frac{qE_G}{kA}\left[\frac{1}{T_{ref}} - \frac{1}{T_c}\right]\right) \quad \text{.....2}$$

In (2),T_{ref} is the cell reference temperature, i_{rr} the reverse saturation current at T_{ref} and E_G the band-gap energy of the cell. The PV current i_{ph} depends on the insolation level and the cell temperature according to

$$i_{ph} = 0.01\left[i_{scr} + K_\theta\left(T_c - T_{ref}\right)\right]S \quad \text{.....3.}$$

In (3), i_{scr} is the cell short-circuit current at the reference temperature and radiation, kθ a temperature coefficient, and S the insolation level in kW/m^2 The power delivered by the PV array is calculated by multiplying both sides of (1) by $v_{pv.}$

$$P_{pv} = n_p i_{ph} v_{pv} - n_p i_{rs} v_{pv}\left[exp\left(\frac{q}{kT_cA}\frac{v_{pv}}{n_s}\right) - 1\right] \quad \text{....4}$$

Substituting from i_{ph} (3) in P_{pv} (4), becomes

$$P_{pv} = 0.01 n_p\left[i_{scr} + K_\theta\left(T_c - T_{ref}\right)\right]S v_{pv} - n_p i_{rs} v_{pv}\left[exp\left(\frac{q}{kT_cA}\frac{v_{pv}}{n_s}\right) - 1\right] \quad \text{....5}$$

Based on (5), it is evident that the power delivered by the PV array is a function of insolation level S at any given temperature. Since the inverter employed in the PV system of this paper is of current-source type, the power-versus-current characteristic of the PV array has to be examined. Fig. 2 illustrates the powerversus- current characteristic of the PV array based on the parameters listed in the Appendix for insolation levels of 0.25,0.5, and 1kW/m^2 . Fig. 2 shows that P_{pv} can be maximized by control of i_{pv} , based on an MPPT strategy[1].

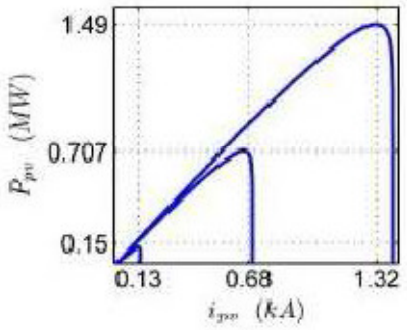

Fig.2.P-I characteristic of a PV array for S=0.25,0.5 and 1kW/m^2

III. DYNAMICS OF CSI-BASED PV SYSTEM

A mathematical model is essential for both system analysis and controller design. In this section, the system of Fig. 1 is modeled in both space-phasor an dq -frame forms.

A .Space-Phasor Representation of the CSI

The CSI of Fig. 1 is a six-pulse converter employing IGBT switches, operated under sinusoidal pulsewidth modulation (SPWM) strategy. The output current of the CSI $\vec{l_t}$ is related to the dc-side current as follows:

$\vec{l_t}$=$\overrightarrow{mi_{dc}}$ 6

where $\vec{l_t}$ and $\overrightarrow{mi_{dc}}$are the space phasors corresponding to the CSI terminal currents and the PWM modulating signals. Similarly, the dc-side voltage is related to the CSI ac-side voltage space phasor as

V_{dc}= $\overrightarrow{mi_{dc}}$ 7

where superscript "T" denotes transposition. Assuming the switching losses of the inverter to be negligible, the dc-side power of the inverter P_{dc} is equal to the power delivered on the ac-side. By power balance principle, one can write

$$P_{dc} \approx P_s = \frac{3}{2}Re\left\{\overrightarrow{v_s}^T\overrightarrow{i_s^*}\right\} \quad \text{.....8}$$

Where * denotes the complex-conjugate operator.

B. DQ-Frame Representation of the PV System....

To simplify the analysis and controller design, the spacephasor variables of the system model are projected on a synchronously rotating dq-frame, where the variables at steady-state assume timeinvariant values. The

relationship between the space phasor and dq-frame variables is expressed by

$$\bar{f}=(f_d + jf_q)e^{j\delta} \qquad (9)$$

Where $\bar{f}$ represents a space phasor variable . $f_d$and f_q are the equalent dq- frames components and δ is the reference angle of the dq – frames .another useful relationship is defined between the derivatives of the space phasor and dq frames variable as follows.

$$\frac{d\bar{f}}{dt} - \frac{d}{dt}[(f_d + jf_q)e^{j\delta}] - \left(\frac{df_d}{dt} + j\frac{df_q}{dt}\right)e^{j\delta} + j\frac{d\delta}{dt}(f_d + jf_q)e^{j\delta} - \left(\frac{df_d}{dt} + j\frac{df_q}{dt}\right)e^{j\delta} + j\omega(f_d + jf_q)e^{j\delta} \qquad \text{…..10}$$

Where ω is the dq –frames angular speed that is related to according to

$\omega = \frac{d\delta}{dt}$ ….11

Based on (9) .P_s in (8) can be expressed as

$$P_s = \frac{3}{2} Re\{[(v_{sd} + jv_{sq})e^{j\delta}][(i_{sd} + ji_{sq})e^{j\delta}]^*\} \qquad \text{..12}$$

Which can be further simplified to

$$P_s = \frac{3}{2}(v_{sd}i_{sd} + v_{sq}i_{sq}) \qquad \text{…….13}$$

The dc-side dynamics can be described by

$$L_{dc}\frac{di_{dc}}{dt} = v_{pv} - v_{dc} \qquad \text{……14}$$

Multiplying both sides of (14)by the current i_{dc} result in the following power relation

$$L_{dc}i_{dc}\frac{di_{dc}}{dt} = v_{pv}i_{dc} - v_{dc}i_{dc} \qquad \text{…..15}$$

The two terms on the right hand side of (15)represent the power delivered by the PV array P_{pv} and the power received by the dc-side of the inverter P_{dc}, respectively. Thus, one can obtain the power balance equation as

$$\frac{1}{2}L_{dc}\frac{d\,i_{dc}^2}{dt} = P_{pv} - P_{dc}(\approx P_s) \qquad \text{…….16}$$

Substituting the expression P_s for from (13) in (16)

Gets

$$\frac{1}{2}L_{dc}\frac{d\,i_{dc}^2}{dt} = P_{pv} - \frac{3}{2}(v_{sd}i_{sd} + v_{sq}i_{sq}) \qquad \text{….17}$$

IV. CONTROLLER FOR CSI-BASED PV SYSTEM

The controller of a grid-connected CSI-based PV system is expected to control the dc- and ac-side currents to ensure:

1) a high-quality sinusoidal current is injected into the grid;

2) the real power injected into the grid is equal to the maximum power that can be extracted from the PV panel under all conditions; and

3) the reactive power at the interface with the grid assumes the desired value. As illustrated by Fig. 1, the pulse width modulation (PWM) and control of the CSI need to be synchronized to the grid voltage through a phase-locked loop (PLL) [2]. Fig. 1 also shows that the errors between the reference commands, i_{sdref} (obtained from MPPT through dcside current controller) and i_{sqref} and the d-axis and q-axis components of the ac-side current are processed by two PI controllers to generate the modulating signals ,m_d and m_q . Even though the PI controller is simple in structure and easy to implement, proper tuning of its parameters requires adequate insight. An intuitive method for tuning of the PI controller parameters is proposed in this section

A. Phase-Locked Loop (PLL)

As discussed earlier, the ac variables of the system are projected on a dq frame which is rotating at angular speed ω. In steady state, the ac variables are sinusoidal functions of the grid frequencyω_0 . If the dq-frame angular speed is adjusted to the grid frequency, the transformed quantities become timeinvariant in steady-state, simplifying the controller design. This is achieved by means of a PLL [2] whose block diagram is given in Fig. 3. As shown in Fig. 3, the input to the PLL block is the sinusoidally varying voltage and the output is the angle for abc - to-dq and dq-to-abc transformations, . The voltage $\vec{v_s}$is resolved into its d- and q-axis components based on (9). In Fig. 3, the voltage v_{sq} is regulated to zero using a PI controller H(s). Regulating the q-axis

component of the voltage to zero makes the active and reactive powers, P_s and Qs , independent of the voltageV_{sq} . From (13)

$$P_{pv} = \frac{3}{2} v_{sd} i_{sd} \quad \text{……..(18)}$$

Hence,P_s is proportional to and can be controlled i_{sd} . Similarly, the dq-frame expression for the reactive power assumes the form

$$Q_s = \frac{3}{2} Im\{\vec{v_s}\vec{i_s}^*\} = \frac{3}{2} Im\{[(v_{sd} + jv_{sq})e^{j\delta}][(i_{sd} + ji_{sq})e^{j\delta}]^*\}$$

$$\frac{3}{2} v_{sd} i_{sq}, \quad (19)$$

Equation (19) indicates that Qs can be controlled by i_{sq}

B. Design of Inner Current Control Loop

Equations (18) and (19) show that active and reactive powers delivered by the CSI can be adjusted by controlling i_{sd} and i_{sq} , respectively. Fig. 4 shows the block diagram of the CSI ac-side current controller.

Controller structures $k_d(S)$and k_q (S) in Fig. 4 are expressed as

$$k_d(s) = k_q(s) = k_p + \frac{k_i}{s} \quad \text{……..20}$$

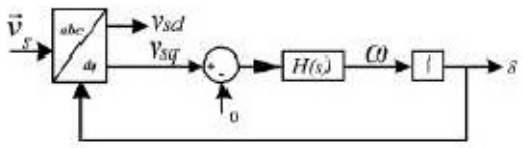

Fig. 3. Block diagram of the PLL

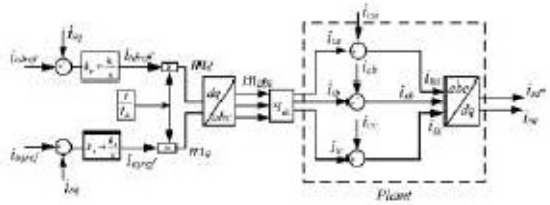

Fig. 4. Block diagram of the CSI ac-side current control system

Where k_p and K_i are the proportional and integral gains, respectively. Control signals m_d and m_q are obtained as

$$m_d = \frac{i_{tdref}}{i_{dc}} \text{ and } m_q = \frac{i_{tqref}}{i_{dc}} \quad \text{……..21}$$

Where i_{tdref} and i_{tqref} are current references derived from the outputs of the compensators $k_d(S)$and $k_q(S)$, respectively. The d-axis component of the inverter output current i_{td} is related to the current i_{sd} as

$$i_{td} = i_{cd} + i_{sd}$$

Where i_{cd} is d-axis component of the filter capacitor current. It should be noted that with a proper filter design, the fundamental frequency component of the capacitor current will be very small, i.e., i_{cd} is negligible as compared to i_{sd} . The same discussion can be made for the q-axis components. Therefore, one can write

$$i_{td} \approx i_{sd} \approx m_d i_{dc} \text{ and } i_{tq} \approx i_{sq} \approx m_q i_{dc} \text{…..23}$$

Under the assumption that i_{cd}=0 the following transfer function can be written for the closed-loop control system of i_{sd} illustrated in Fig. 4

$$T(s) = \frac{i_{sd}}{i_{sdref}} = \frac{k_p + \frac{k_i}{s}}{k_p + \frac{k_i}{s} + 1} = \frac{s\frac{k_p}{k_p+1} + \frac{k_i}{k_p+1}}{s + \frac{k_i}{k_p+1}} \quad (24)$$

As the value of k_p increases, the pole of the transfer Function T(S) in (24) approaches the origin of splane, which is not desirable. Therefore, to imitate the transient behavior of a first-order system, k_p should be chosen to be small.k_i , as the inverse of time constant,τ_i is chosen in the range of 0.5–5 ms to get a fast and accurate response. Thus,k_p and $k_i$can be written as

$$k_p = 0 \text{ and } k_i = \frac{1}{\tau_i} \quad \text{……..25}$$

Substituting the values of k_p and k_i in (24), the transfer function T(S) becomes

$$T(s) = \frac{i_{sd}}{i_{sdref}} = \frac{\frac{1}{\tau_i}}{s + \frac{1}{\tau_i}} = \frac{1}{\tau_i s + 1} \quad (26)$$

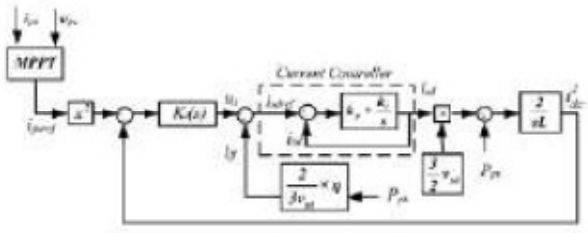

Fig. 5. Closed-loop control structure of the dc-side current

C. Design of Outer Current Control Loop

Equation (17), after substituting v_{sq}=0 , represents a system with i_{sd} as the input i_{dc}^2 the output and V_{sd} the disturbance input. If time constant $\tau_i$in the PI compensator of the current controller is properly selected,

i_{sd} can be approximated to i_{sdref} . Therefore, (17) can be rewritten as

$$\frac{1}{2}L_{dc}\frac{di_{dc}^2}{dt} \approx P_{pv} - \frac{3}{2}v_{sd}i_{sdref} \qquad (27)$$

The dc-link current controller designed on the basis of (27) is illustrated in Fig. 5. According to (27), the fact that p_{pv} is product of v_{pv} and i_{dc} makes the system nonlinear. To mitigate the impact of nonlinearity,i_{sdref} can be derived in the following way:

$$i_{sdref} = u_i + n\left(\frac{P_{pv}}{\frac{3}{2}v_{sd}}\right) \qquad (28)$$

Where $\mu_i$is a new control input, shown in Fig. 5 and $i_{ff}$is a feed-forward signal that can be enabled or disabled when the binary multiplier n assumes the value unity or zero. Substituting for i_{sdref} from (28) in (27), one gets

$$\frac{L_{dc}}{2}\frac{di_{dc}^2}{dt} \approx (1-n)P_{pv} - \frac{3}{2}v_{sd}u_i$$

Equation (29) indicates that if =1 , the impact of the PV array nonlinearity on the dc-side current control is eliminated and the effective control unit becomes an integrator

V. COMPARATIVE PERFORMANCE EVALUATION OF THE CSI-BASED PV SYSTEM WITH THE VSI-BASED PV SYSTEM

The objective of this section is to evaluate the performance of the CSI-based PV system in comparison with that of a VSI based PV system. The results for VSI-based PV system are produced by simulating the system presented in [3]

A. Case Study 1: Change in Insolation Level

In this case study, the behaviors of the VSI- and CSIbased PV systems in response to a change in insolation level are illustrated. Since VSI and CSI are dual topologies, the characteristic of voltage in CSI is analogous to that of current in VSI and vice versa. Initially, the insolation level is set to 0.4 kW/m^2 . At t=1s, the insolation level is step-changed to 0.6 kW/m^2 , as shown in Fig. 6(a). With the change in insolation level, the CSI dc-side current reference changes from 0.7 to 1 kA by the MPPT tracker. The new reference is tracked by the outer current control loop or the dc-side current controller, as shown in Fig. 6(b). Since the terminal current of the CSI i_t is linearly related to the dc-side current i_{dc}, it is also changed as shown in Fig. 6(c).

The ac-side reference current is derived from the dcside current control loop. Since there is an increase in the dc-side current, the d-axis current reference i_{sdref} increases and so does the current i_{sd} , as shown in Fig. 7(a). With the increase in i_{ga} , the current on the secondary side of the transformer also increases. The utility mandates that the current injected by the inverter i_{ga} be in-phase with the voltage at the PCC.

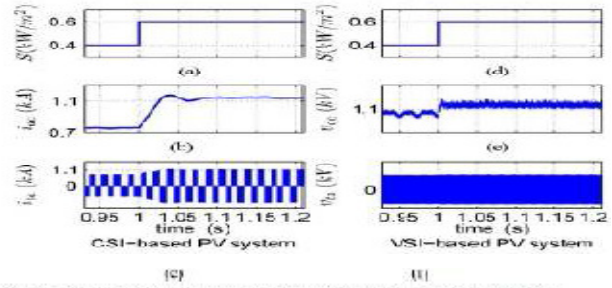

Fig. 6. PV system behavior in response to a step-change in insolation level for CSI- and VSI-based PV systems. (S = Insolation level; i_{dc} = dc-side current of CSI; v_{dc} = dc-side voltage of VSI; i_{ga} = Phase-a ac terminal current of CSI; v_{ta} = Phase-a ac terminal voltage of VSI).

This is shown in Fig. 7(b). Figs. 6(d)–(f) and 7(b)–(d) show the performance of a VSI-based PV system in response to the same step change in insolation level. One can observe in Fig. 6(e) a step change in the dcside voltage level of the VSI as a result of a change in insolation level, similar to that in dc-side current of CSI. The ac-side terminal voltage of VSI, shown in Fig. 6(f), is a two-level quantity whereas the ac-side terminal current of CSI is a three-level quantity. Fig. 7(c) illustrates the filtered output voltage of the VSI. The unity power factor maintained by the VSI-based PV system at the PCC is illustrated in Fig. 7(d). From this case study,it can be inferred that the performance of the CSI-based PV system is quite satisfactory and even superior to that of VSI-

based PV system due to three-level output current (as compared to two-level output voltage of VSI), simpler ac-side filter design and direct control of injected current (as compared to indirect output current control in VSI)

B. Case Study 2: Fault Conditions

Fault on the grid-side of the inverter results in oscillations of current and voltage on the dc-side of the inverter [4]. Oscillations in the dc-side current are not desirable as the inverter requires a smooth input dc-current. In case of VSI-based PV system, the controller regulates the dc-side voltage; therefore, there is no direct control on the dc-side current. On the contrary, in CSI-based PV system, the dc-side current is regulated and limited. As a result, the current on the ac-side of the inverter may

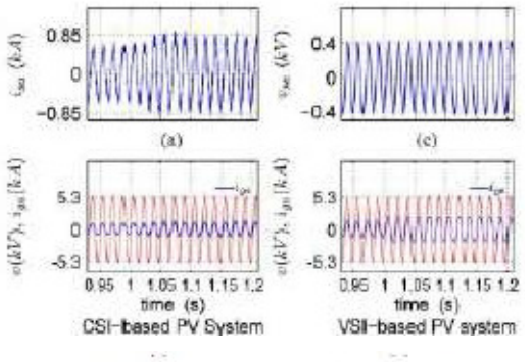

Fig. 7. PV system behavior in response to a step-change in insolation level for CSI- and VSI-based PV systems. (i_{sa} = CSI phase-a filtered current injected into the grid; v_{sa} = VSI phase-a filtered voltage at the grid interface; v = CSI voltage at the PCC, i_{ga} = phase-a current at the PCC).

not show a sharp rise under fault. This case study is designed to present a comparative analysis of behaviors during fault for CSI- and VSI-based PV systems. For this study, the insolation level is maintained at 1 kW/ m^2. In real life, when the fault occurs on the grid-side and the breaker Br opens, the anti-islanding scheme must act to protect the inverter and personnel. Since the objective of this case study

is to show the impact of a change in the ac-side voltage level on the performance of the PV system, the anti islanding protection is disabled. Four fault types, i.e., single line-to-ground (SLG), double lineto- ground (DLG), line-to-line (LL), and three-phaseto- ground (TPG) are studied.

At time t=1.5s, an SLG fault is applied on phase-a of secondary side of the transformer Tr. Due to the fault, the voltage Va drops to zero, as shown in Fig. 8(a). Application of fault on the ac-side has resulted in oscillations in the dc-side current of the CSI, as shown in Fig. 8(b). However, oscillations are damped as soon as the fault is cleared and the dcside current controller tracks the reference current in less than 20 ms. Due to this disturbance, the ac terminal current of the CSI undergoes over modulation, as shown in Fig. 8(c). The over modulation results in low order harmonics and the current i_{sa} injected into the grid is no longer sinusoidal, as shown in Fig. 8(d). This case study clearly shows the inherent over-current protection built in CSI that limits the currents on both dc and ac sides. Similar responses are observed for DLG, LL, and TPG faults, as illustrated in Figs. 8(e)–(h), 9(a)– (d) and 9(e)-(h) respectively. In all types of faults, the magnitude of the sinusoidal current injected into the grid is limited. The reason for penetration of low order harmonics in the grid during the fault in the presence of filter C_f is that capacitor is designed to filter out the switching harmonics, not low-order harmonics.

Harmonic spectrums of the terminal current and the current injected into the grid before and during an SLG fault are shown in Fig. 10. Figs. 10(a) and (b), respectively, illustrate the harmonic spectrums of i_{ta} and i_{sa} before the fault. It is clear that before the fault there are no major low-order harmonics and the switching harmonics are filtered out in the current i_{sa}. Fig. 10(c) illustrates the harmonic spectrum of the current i_{ta} during the fault. The harmonic spectrum of the current i_{sa} during the fault given by Fig. 10(d) shows that the capacitor has not been able to filter out the low-order harmonics.

Fig. 11 illustrates the performances of CSIand VSI-based PV systems during an SLG fault. As mentioned earlier, in the VSI-based PV system, the controller on the dc-side is

employed to control the dc-side voltage, whereas in the CSI-based PV system, the controller's task is to control the dc-side current during fault, whereas the ac-side current of VSI shows a sharp rise in the presence of a current limiter, as illustrated by Fig. 11(d).

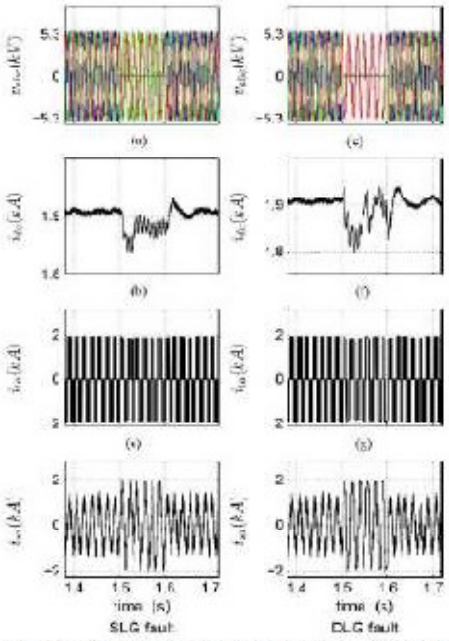

Fig. 8. CSI-based PV system performance during SLG and DLG faults (v_{abc} = three phase voltage on the secondary side of T_r; i_{dc} = dc side current of the CSI; i_{ta} = phase a terminal current of CSI; i_{sa} = phase a current injected to the grid).

Fig. 10. Harmonic spectrum of CSI's ac terminal and filtered currents before and during fault . One can observe from Fig. 11(a) that the range of variation in the dc-side current of CSI during fault is tightly limited due to the regulatory role of the dcside current controller. On the contrary, Fig. 11(c)shows that the dc-side current of VSI is allowed to vary in a wide range. Also, Fig. 11(b) shows that the amplitude of CSI's ac-side current is limited during fault, whereas the ac-side current of VSI shows a sharp rise in the presence of a current limiter, as illustrated by Fig. 11(d).

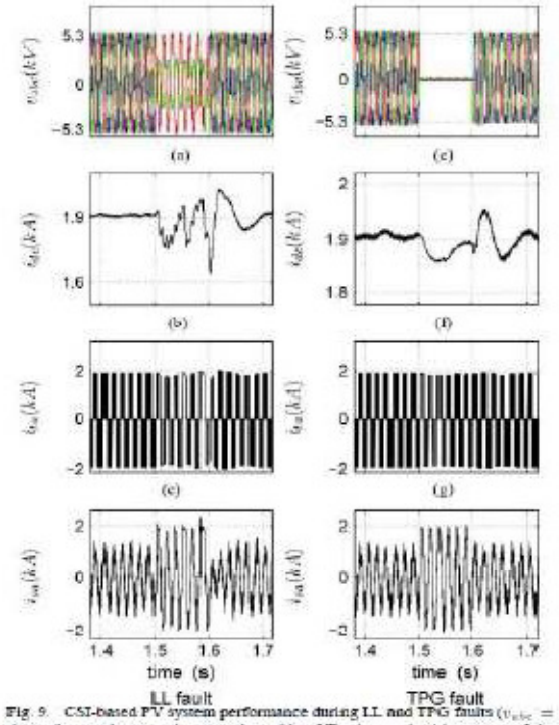

Fig. 9. CSI-based PV system performance during LL and TPG faults (v_{abc} = three-phase voltage on the secondary-side of T_r; i_{dc} = dc-side current of the CSI; i_{ta} = phase-a terminal current of CSI; i_{sa} = phase-a current injected to the grid).

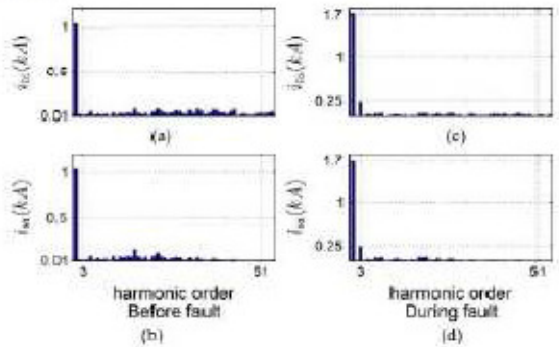

Fig. 10. Harmonic spectrum of CSI's ac terminal and filtered currents before and during fault

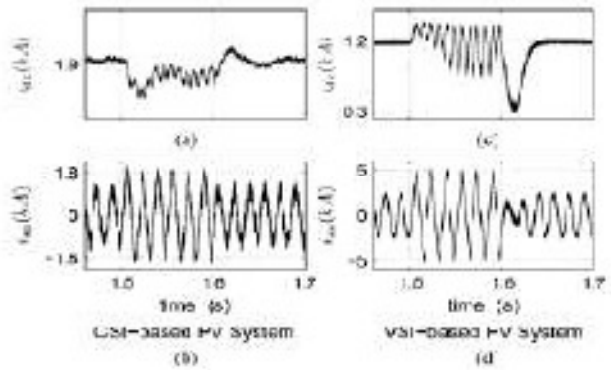

Fig. 11. PV system's performance during SLG fault

VI. CONCLUSION

The paper presented a dynamic model and a control structure for a single-stage, three-phase gridconnected PV system based on CSI. The control structure consists of two current control loops. An MPPT provides the reference for the outer dc-side current control loop. The inner current control loop is designed to control the current that is injected into the grid. Using two case studies, i.e., a step change in insolation level and a grid-side fault, a comparative performance evaluation of CSI- and VSI based PV systems was performed. The fault studies included single-phase-to-ground, two-phase-to-ground, line to- line, and three-phase-to-ground faults. Through simulation studies, it was shown that the CSI-based PV system, with the designed controller, was able to fulfill all the requirements of a PV system grid interface beside limiting the dc-side current

APPENDIX
SYSTEM PARAMETERS

TABLE I
SYSTEM PARAMETERS

PV System Parameter	Value	Comments
Grid inductance, L_g	1 mH	
Grid Resistance, R_g	1 $m\Omega$	
Grid voltage, v_g	6.6 kV	
T_r nominal power	1.3 MVA	
T_r voltage ratio	6.6/0.48 kV	Delta/Y
T_r leakage inductance	0.1 pu	
T_r ohmic resistance	0.02 pu	
on-state resistance of valves, R	3 $m\Omega$	
filter capacitance, C_f	300 μF	
switching frequency	3060 Hz	51×60 Hz
DC-link capacitance, C	5000 μF	
DC-link inductance, L_{dc}	1 mH	
# of PV cells per string, n_s	1500	
# of PV strings, n_p	176	
ideality factor, A	1.92	
cell reference temperature, T_{ref}	300 K	
temperature coefficient, k_0	0.0017 A/K	
cell short circuit current, I_{scr}	8.03 A	
reverse saturation current, I_{rs}	1.2×10^{-7} A	
Controller Parameter	**Value**	**Comments**
k_p (for $\tau_i = 0.5$ ms)	0.0002	
k_i (for $\tau_i = 0.5$ ms)	2 s^{-1}	

REFERENCES

[1] K. H. Hussein, I. Muta, T. Hoshino, and M. Osakada, "Maximumphotovoltaic power tracking: an algorithm for rapidly changing atmosphericconditions," in *IEEE Proc. Generation, Transmission andDistribution*, 1996, pp. 1752–1757.

[2] S. K. Chung, "A phase tracking system for three phase utility interfaceinverters," *IEEE Trans. Power Electron.*, vol. 15, no. 3, pp. 431–438,2000.

[3] A. Yazdani and P. P. Dash, "A control methodology and characterizationof dynamics for a photovoltaic (PV) system interfaced with adistribution network," *IEEE Trans. Power Delivery*, vol. 24, no. 3, pp.1538–1551, Jul. 2009.

[4] C. Photong, C. Klumpner, and P. Wheeler, "A current source inverterwith series connected ac capacitors for photovoltaic application withgrid fault ride through capability," in *Proc. Industrial*